ACS APPLIED MATERIALS & INTERFACES

Research Article

www.acsami.org

Multifunctional Polymeric Platform of Magnetic Ferrite Colloidal Superparticles for Luminescence, Imaging, and Hyperthermia Applications

Zacharoula Iatridi,[†] Kosmas Vamvakidis,[‡] Ioannis Tsougos,[§] Katerina Vassiou,[∥] Catherine Dendrinou-Samara,*[,‡] and Georgios Bokias*[,†,⊥]

[†]Department of Chemistry, University of Patras, GR-26504 Patras, Greece

[‡]Department of Chemistry, Aristotle University of Thessaloniki, GR-54124 Thessaloniki, Greece

[§]Department of Medical Physics, University Hospital of Larissa, University of Thessaly, Biopolis, GR-41110 Larisa, Greece

[∥]Department of Radiology, University Hospital of Larissa, University of Thessaly, Biopolis, GR-41110 Larisa, Greece

[⊥]FORTH/ICE-HT, Stadiou Street, P.O. Box 1414, GR-26504 Rio-Patras, Greece

Supporting Information

ABSTRACT: Adequately designed multiresponsive water-soluble graft copolymers were used to serve as a multifunctional polymeric platform for the encapsulation and transfer in aqueous media of hydrophobic magnetic nanoparticles (MNPs). The backbone of the graft copolymers was composed of hydrophilic sodium methacrylate units, hydrophobic dodecyl methacrylate units, and luminescent quinoline-based units, while either the homopolymer poly(*N*-isopropylacrylamide) or a poly(*N*,*N*-dimethylacrylamide-*co*-*N*-isopropylacrylamide) copolymer was used as thermosensitive pendent side chains. The polymeric platform forms micellar-type assemblies in aqueous solution, and exhibits pH-responsive luminescent properties and a lower critical solution temperature behavior in water. Depending on the design of the side chains, the cloud point temperatures were determined at 38 and 42 °C, close or slightly above body temperature (37 °C). Above the critical micelle concentration (CMC), both graft copolymers can effectively stabilize in aqueous media as magnetic colloidal superparticles (MSPs), oleylamine-coated $MnFe_2O_4$ MNPs, as well as 1:1 mixture of oleylamine-coated $MnFe_2O_4$ and $CoFe_2O_4$ MNPs. When $CoFe_2O_4$ particles were mixed with $MnFeO_4$ in equal amounts, the specific loss power increased significantly, while an opposite trend was observed in the magnetic resonance imaging (MRI) studies, probably due to the anisotropy of cobalt. As a consequence, fine-tuning of the chemical structure of the copolymers and the composition of the MSPs can lead to materials that are able to act simultaneously as luminescent, hyperthermia, and contrast MRI agents.

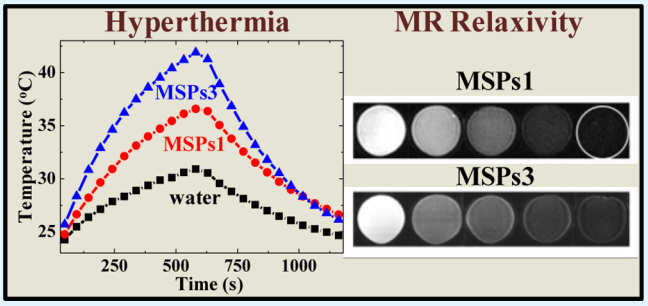

KEYWORDS: *graft copolymers, hydrophobically modified water-soluble polymers, poly(N-isopropylacrylamide), luminescent labeling, magnetic nanoparticles, hyperthermia, magnetic resonance imaging*

1. INTRODUCTION

A main goal of recent research for biomedical applications is the design of novel multifunctional "smart" systems, which integrate therapeutic and diagnostic capabilities (theranostics).[1] Emerging technologies in preparation of magnetic nanoparticles (MNPs)[2,3] have rendered hybrid MNP-based nanoarchitectures as suitable and versatile platforms for applications targeting potentially combined treatment, diagnosis, monitoring, and control of biological systems. In fact, such hybrid MNPs offer the advantage of combining multiple functions and exploiting possible synergies such as magnetic resonance imaging (MRI), hyperthermia, and drug loading and delivering, while additional functionalities may be incorporated, like responsiveness to stimuli or luminescence.[4−10]

Single-crystal inorganic magnetic nanoparticles (MNPs) have attracted considerable attention over the past decade particularly for biological and medical applications, comprising the first generation of nanomaterials.[11−17] Significant progress has been made in the development of reliable synthetic protocols, which offer precise control over size, polydispersity, shape, composition, and surface properties in order to improve the performance of the produced particles.[18] Recently, the focus of scientists has been directed toward the creation of superstructures, as the second generation of nanomaterials, namely, magnetic colloidal superparticles (MSPs),[19] were

Received: October 16, 2016
Accepted: December 1, 2016
Published: December 1, 2016

DOI: 10.1021/acsami.6b13161
ACS Appl. Mater. Interfaces 2016, 8, 35059−35070

Scheme 1. Schematic Depiction and Synthetic Methodology for the Preparation of the P(MANa-*co*-DMA-*co*-SDPQ)-*g*-P(DMAM-*co*-NIPAM) Copolymer[a]

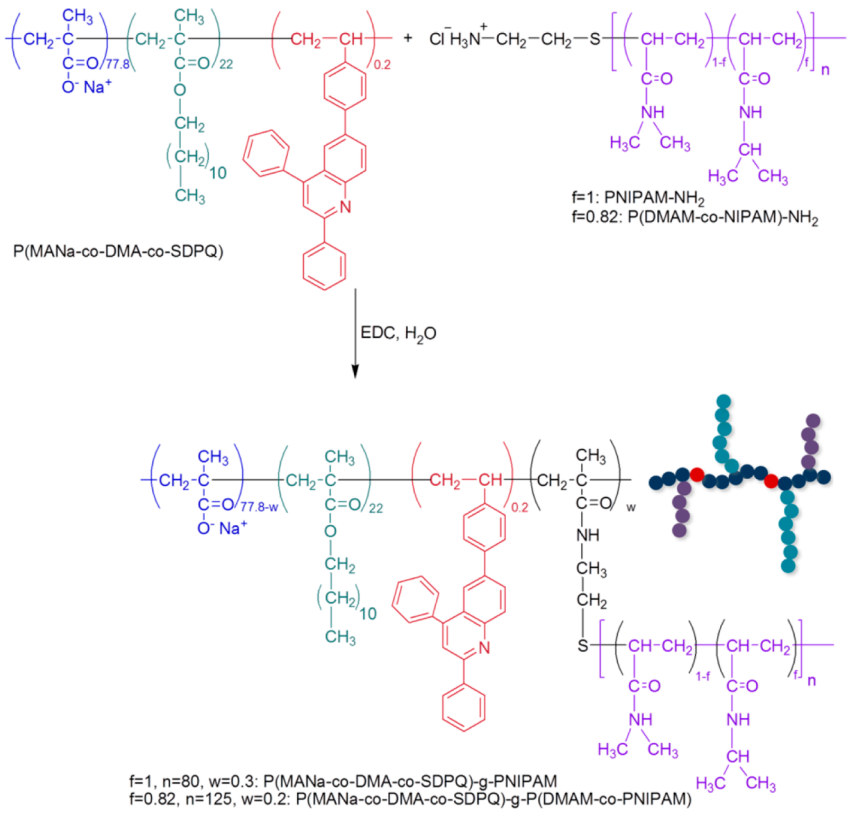

[a]When the amine-terminated PNIPAM-NH_2 is used, the P(MANa-*co*-DMA-*co*-SDPQ)-*g*-PNIPAM graft copolymer is obtained. The values of *n* and *w* are calculated from the number-average molar masses, M_n, of the side chains (*n*), in combination with the molar composition of the final products (*w*), reported in Table 1.

constructed from individual nanocrystals. Self-assembly organization of single nanoparticles can result in enhanced magnetic performance emerging from the interactions between neighboring particles.[20−23] An effective way to stabilize MNPs in water, especially hydrophobic ones, and create MSPs is their encapsulation in polymeric nanostructures. A variety of polymers with different architectures like block[24−26] or hydrophobically modified water-soluble (HMWSP)[27−31] copolymers have been utilized for the dispersion of hydrophobic MNPs in water.

Stimuli-responsive polymers have attracted significant scientific interest in biomaterial science and technology because their properties can be adjusted in a controlled manner.[32] These are polymers that change their structure and physical characteristics in response to external stimuli such as temperature, pH, light, ionic strength, etc. Among all external stimuli, pH and temperature are the most popular and mostly studied in the field of targeted delivery and therapy. Recently, dual responsive or thermoresponsive polymer-coated MNPs have been used for targeted drug delivery and hyperthermia treatment. While pH responsiveness is based on the use of weakly acidic or basic units, the well-known behavior of poly(*N*-isopropylacrylamide) (PNIPAM) is usually exploited to achieve the thermoresponsiveness.[6,8,9,33−38] PNIPAM is a thermosensitive polymer that exhibits a lower critical solution temperature (LCST) phase-transition behavior in aqueous solution at around 32 °C.[39−42] PNIPAM is soluble in the aqueous phase and takes an expanded form below LSCT, while above LCST it becomes hydrophobic and undergoes reversible volume shrinkage due to the expulsion of water from its chains. The LCST of PNIPAM can be precisely adjusted close to body temperature by copolymerizing NIPAM with hydrophilic monomers, thus making it suitable for applications involving drug delivery, hyperthermia, etc. For such applications, either the direct coating of MNPs with adequate NIPAM-based copolymers[5,8,9,37,43] or designed block copolymers[6,24,35] have been mostly proposed.

Our groups focus on the development of oleylamine-coated MFe_2O_4@OAm MNPs (where M = Co, Mn, Ni) using a solvothermal route and their potential bioapplications.[44−46] Recently we studied the ability of hydrophobically modified water-soluble copolymers with comb-type or linear architecture to act as potential encapsulating polymeric agents for the hydrophilization of hydrophobic MFe_2O_4@OAm (where M = Co, Mn, Ni) ferrites. Some of the studied systems exhibited promising properties for potential use as T_2 contrast agents. For example, the hydrophobically modified copolymer P(MANa-*co*-DMA) composed of a poly(sodium methacrylate) backbone and pendent dodecyl methacrylate chains has been proven to be an effective agent for the transfer of hydrophobic MFe_2O_4@OAm ferrites (where M = Co, Mn, Ni) in water. This successful water dispersion is achieved by the characteristic self-organization behavior of P(MANa-*co*-DMA); these species form micelle-like supramolecular structures with a DMA hydrophobic core encapsulating the hydrophobic iron ferrites

DOI: 10.1021/acsami.6b13161
ACS Appl. Mater. Interfaces 2016, 8, 35059−35070

Table 1. Physicochemical Characterization Results of the Amphiphilic Copolymers Used in the Present Work

side chains	comp (% mol in NIPAM)[a]	M_n (g/mol)[b]	T_{CP} (°C)[d]
PNIPAM-NH_2	100	9000	35
P(DMAM-*co*-NIPAM)-NH_2	82	14000	38

copolymer	% moles of the respective units (calculated from ^{1}H NMR)[a]				CMC (wt %)	T_{CP} (°C)[d]
	MANa	DMA	SDPQ	side chain		
P(MANa-*co*-DMA-*co*-SDPQ)	77.8	22.0	0.2		0.002[c]	
P(MANa-*co*-DMA-*co*-SDPQ)-*g*- PNIPAM	59.0	16.8	0.2	24.0	0.002[c]	38
P(MANa-*co*-DMA-*co*-SDPQ)-*g*- P(DMAM-*co*-NIPAM)	56.4	16.0	0.2	27.4	0.002[c]	42

[a]From ^{1}H NMR. [b]From acid−base titration. [c]Determined through Nile Red probing from the respective copolymers without SDPQ. [d]From turbidimetry.

and a hydrophilic MANa corona that stabilizes the nanostructure in aqueous solution.

In the present work we design a much more ambitious system for the dispersion of hydrophobic oleylamine-coated $MnFe_2O_4$ ferrites in water, in order to introduce multiresponsive properties as well as other functionalities (luminescence). In addition, apart from single $MnFe_2O_4$ ferrites, the same procedure was applied to stabilize assemblies of $MnFe_2O_4$ and $CoFe_2O_4$ ferrites in order to enhance the magnetic properties for different detection modalities (MRI and hyperthermia). As far as we are aware, such mixed systems have not been reported. For this purpose, we synthesized dual responsive (pH and temperature) copolymers comprising a luminescent hydrophobically modified polymeric backbone, grafted with thermoresponsive side chains. The general structure of the copolymers used is presented in Scheme 1. The backbone of the graft copolymers, poly(sodium methacrylate-*co*-dodecyl methacrylate-*co*-2,4-diphenyl-6-(4-vinylphenyl)quinoline) (P(MANa-*co*-DMA-*co*-SDPQ)), is basically a hydrophobically modified water-soluble terpolymer bearing carboxylic groups (MANa), hydrophobic dodecyl chains (DMA), and luminescent quinoline groups (SDPQ). Quinoline groups are characterized by their weak basic character and their protonation/deprotonation behavior in the change of the emitted color from blue to green upon decreasing pH.[47,48] Moreover, it has been recently demonstrated in our lab that water-soluble quinoline-labeled polymers or cross-linked organic nanoparticles with pH-controlled luminescent[49,50] and sensing[51,52] properties can be easily synthesized and studied in water. The grafted side chains are thermoresponsive poly(*N*-isopropylacrylamide) (PNIPAM) or poly(*N*,*N*-dimethylacrylamide-*co*-*N*-isopropylacrylamide) (P(DMAM-*co*-NIPAM)) with different LCSTs. Hyperthermia study and MRI measurements at 1.5 T proved that the materials could be promising candidates for relevant theranostic treatments (magnetic hyperthermia-imaging agents). To our knowledge, graft polymeric architectures like those presented in Scheme 1 have not yet been exploited for such applications, though they represent an easily adaptable and versatile synthetic methodology, as compared to the synthetic implications (for example, use of special initiators and/or metal complexes, strict purity, or reaction conditions, etc.) often faced with the block copolymer strategy in some cases.

2. MATERIALS AND METHODS

2.1. Materials. The monomer methacrylic acid (MAA) and the fluorescent probe Nile Red were purchased from Fluka. The monomer dodecyl methacrylate (DMA) was obtained from Acros. The monomer *N*,*N*-dimethylacrylamide (DMAM), the chain transfer agent 2-aminoethanethiol hydrochloride (AET, HCl), and the coupling agent 1-ethyl-3-(3-dimethylamino propyl) carbodiimide hydrochloride (EDC) were obtained from Alfa Aesar and used as received. The monomer *N*-isopropylacrylamide (NIPAM), the initiators azobis(isobutyronitrile) (AIBN) and ammonium persulfate (APS), and the solvents tetrahydrofuran (THF), petroleum ether and deuterated water (D_2O) were all purchased from Aldrich. The reagents for the preparation of the buffer solutions, trisodium citrate dihydrate and hydrochloric acid, were purchased from Merck. The buffer solutions were prepared by adequate mixing of a 0.1 M trisodium citrate dihydrate aqueous solution with a 0.1 M hydrochloric acid solution. 2,4-Diphenyl-6-(4-vinylphenyl)quinoline (SDPQ) was prepared according to literature procedures.[53] Ultrapure 3D-water was obtained by means of an SG Waters apparatus.

2.2. Synthesis of the P(MANa-*co*-DMA-*co*-SDPQ) Backbone. A THF solution of the monomers MAA, DMA, and SDPQ and the initiator AIBN was added in a three-neck round-bottom flask equipped with a reflux condenser. The MAA/DMA molar ratio was set at 4/1, while the quantities of SDPQ and AIBN were 0.2% and 0.015% over the total monomer concentration. The mixture was degassed with Ar for 2 h, and the reaction was performed by heating at 70 °C and was left overnight under stirring. The polymer was recovered through precipitation in petroleum ether and dried under vacuum at 40 °C. The acid form of the copolymer, P(MAA-*co*-DMA-*co*-SDPQ), was transformed into the sodium salt form, P(MANa-*co*-DMA-*co*-SDPQ), through dissolution in an aqueous NaOH solution. The copolymer was purified through dialysis against pure water (membrane cutoff: 12 kDa) and lyophilization. For reasons of comparison, the backbone P(MANa-*co*-DMA) without the SDPQ moieties was also prepared following the same synthetic procedure.

2.3. Synthesis of PNIPAM-NH_2. The polymerization reaction was accomplished following the method proposed by Durand and Hourdet.[54] Briefly, amine-terminated PNIPAM chains were synthesized through free radical telomerization in water at 29 °C using APS and AET as initiator and telogen, respectively. The monomer concentration was 1 M, while the molar concentrations of APS and AET were adjusted at 2% and 1% over the monomer concentration, respectively. The solution was left under stirring and under argon at room temperature for 24 h. The final homopolymer was recovered by dialysis against pure water (membrane cutoff: 12 kDa) and lyophilization. The amine-terminated PNIPAM chains (PNIPAM-NH_2) were characterized by ^{1}H NMR and acid−base titration, and the number-average molecular weight was determined to be 9000 (Table 1).

2.4. Synthesis of P(DMAM-*co*-NIPAM)-NH_2. The same procedure as described for PNIPAM-NH_2 was used for the synthesis of the P(DMAM-*co*-NIPAM)-NH_2 random copolymer. In this case, an aqueous solution containing both monomers DMAM and NIPAM was prepared. The final concentration of monomers was 10 wt %, while the feed composition used was 18% mol DMAM and 82% mol NIPAM (Table 1).

2.5. Synthesis of Graft Copolymers. The PNIPAM-NH_2 and P(DMAM-*co*-NIPAM)-NH_2 side chains were grafted onto the carboxylic groups of the P(MANa-*co*-DMA-*co*-SDPQ) copolymer in

DOI: 10.1021/acsami.6b13161
ACS Appl. Mater. Interfaces 2016, 8, 35059−35070

aqueous solution and at room temperature, using EDC as a condensing agent. The side chain/backbone mass ratio was set at 0.25/1. The mixtures were left under gentle stirring for 3 days, while a quantity of 0.1 g of EDC was added daily. Afterward, the solutions were fully neutralized with a large excess of NaOH, and the final products, P(MANa-*co*-DMA-*co*-SDPQ)-*g*-PNIPAM and P(MANa-*co*-DMA-*co*-SDPQ)-*g*-P(DMAM-*co*-NIPAM), were recovered by lyophilization, after purification through dialysis with 3D water (membrane cutoff: 12 kDa). For reasons of comparison, two graft copolymers without the SDPQ units, namely, P(MANa-*co*-DMA)-*g*-PNIPAM and P(MANa-*co*-DMA)-*g*-P(DMAM-*co*-NIPAM), were prepared using the backbone P(MANa-*co*-DMA).

2.6. Preparation of Magnetic Colloidal Superparticles MFe_2O_4@polymer. Hydrophobic manganese and cobalt ferrite nanoparticles coated with oleylamine were synthesized following the solvothermal method published previously by our group.[45,46] Aqueous solutions of P(MANa-*co*-DMA-*co*-SDPQ)-*g*-PNIPAM and P(MANa-*co*-DMA-*co*-SDPQ)-*g*-P(DMAM-*co*-NIPAM) at specific polymer concentrations were prepared in 3D water and left under stirring overnight. A small volume of a THF dispersion of $CoFe_2O_4$@OAm, $MnFe_2O_4$@OAm, or a mixture (1:1) of $CoFe_2O_4$@OAm and $MnFe_2O_4$@OAm MNPs was added in the aqueous polymer solutions. The polymer/MNPs mixing ratio was adjusted to 10/1 by weight. The mixtures were sonicated in a Branson 1510 70 W, 40 kHz sonicator and then left at 40 °C until full evaporation of THF.

2.7. Characterization Techniques. ^{1}H NMR spectra of the synthesized polymers in D_2O were obtained on a Bruker Advance DPX 400 MHz spectrometer. The number-average molar mass of the thermosensitive side chains PNIPAM-NH_2 and P(DMAM-*co*-NIPAM)-NH_2 was determined by acid−base potentiometric titration of the end groups using aqueous NaOH 0.1 M and HCl 0.01 M solutions.

2.8. Turbidimetry. For the detection of cloud point temperature (T_{CP}), the optical density at 500 nm was measured using the HITACHI U-1800 UV−vis spectrophotometer equipped with a circulating water bath that allows accurate control of temperature. The polymer solutions were placed in a 10 mm path length quartz cuvette.

2.9. Photoluminescence (PL) and Nile Red Fluorescence Probing. Photoluminescence spectra (PL) of the copolymers or Nile Red probe in aqueous solutions were recorded on a PerkinElmer LS50B luminescence spectrometer. The excitation and emission slits were fixed at 10 nm. For Nile Red fluorescence probing, a small volume (5 μL) of a stock THF solution, containing 1×10^{-3} M Nile Red, was added in 3 mL of the aqueous polymer solution. The final concentration of the probe was, thus, fixed at 1.7×10^{-6} M. The maximum intensity of the emission peak of Nile Red in the region 600−650 nm, after excitation at 550 nm, was used to detect the formation of hydrophobic microdomains. To detect the luminescence of the quinoline-labeled copolymers, the excitation wavelength was set at 350 nm.

2.10. Transmission Electron Microscopy (TEM). TEM experiments were carried out using a JEM 2100 microscope operating at 200 kV. Aqueous dispersions were used for the TEM investigation of the colloidal superparticles.

2.11. Scanning Electron Microscopy (SEM). The elemental composition of the samples was tested by SEM JEOL 840A, where energy dispersive X-ray spectrometry (EDS) spectra were obtained.

2.12. Magnetic Hyperthermia Measurements. Heating experiments were performed in an arrangement using a water-cooled induction coil of 23 mm diameter consisting of three turns, producing an alternating magnetic field (AMF) with a frequency of 765 kHz and an amplitude of 250 Oe (20 kA m^{-1}). The ac field was generated by means of a commercial generator with a power of 4.5 kW. Temperature was monitored with a fiber optic probe placed in the center of the heated vial. During measurement, heating and natural cooling sequences were recorded, each of them, for about 600 s. SLP values were extracted from the initial slope of the heating curve before the interference of heat conduction becomes significant.[55] In order to extract a more accurate SLP value, the reference signal corresponding to the solvent was subtracted from the measured data, while the thermal losses to the environment were also considered in the SLP estimation.[56] For all measurements, a 1 mL portion of aqueous superparticle dispersion was used and subjected to the external field. Temperature data for these experiments were obtained using a fiber optic temperature probe. The heating capacity of the superparticles was quantified by the specific loss power (SLP), defined as the amount of energy converted into heat per time and mass. The SLP is calculated using the following relation:

$$\mathrm{SLP} = C_\mathrm{p}\frac{m_\mathrm{f}}{m_\mathrm{NPs}}\frac{\Delta T}{\Delta t}$$

Here, the following abbreviations apply: C_p is the specific heat of the solution, m_f is the sample volume, m_{NPs} is the mass of magnetic material in the sample, and $\Delta T/\Delta t$ is the initial slope of the heating curve.

2.13. MR Relaxivity Measurement. The longitudinal (T1) and transverse (T2) relaxation time measurements at different concentrations (0.0125−0.8 mM) of the metal ions were performed on a clinical MRI Scanner (a 1.5 T Siemens Aera) using a Head/Neck coil. The T1-weighted images were obtained by an inversion recovery (IR) T1 pulse sequence with variable inversion values (IR = 25−4000 ms) and an echo time (TE) of 12 ms (1.5 T)/43 ms (3 T). Imaging parameters were as follows: 1.5 T, field of view (FOV) = 250.250 mm^2, matrix size (MTX) = 128.128, number of axial slices = 1, slice thickness = 20 mm, and number of averages (NEX) = 1. T2-weighted images were obtained by a multiecho spin−echo T2 pulse sequence (5 echoes; 25−50−75−100−125 ms, and static TR (2000 ms). Imaging parameters were as follows: 1.5 T, FOV = 250 × 250 mm^2, MTX = 256 × 128, number of axial slices = 1, slice thickness = 5.0 mm, and NEX = 1. The resulting set of images was processed off line using an image sequence analysis tool developed in IDL (IDL 8.2, Boulder, CO). T1 and T2 analyses were carried out by fitting a monoexponential curve on the image intensities measured on the selected regions of interest (ROIs) for each axial slice.

3. RESULTS AND DISCUSSION

3.1. Synthesis of Copolymers and Multifunctionality in Aqueous Solution. The general chemical procedure for the synthesis of the polymer products is presented in Scheme 1. As mentioned, the backbone of the graft copolymers, P(MANa-*co*-DMA-*co*-SDPQ), is basically a hydrophobically modified water-soluble copolymer bearing carboxylic and quinoline groups, as well as dodecyl side chains. This polymer has been synthesized through free radical copolymerization (FRP) of MAA, DMA, and SDPQ, followed by neutralization of the polyacid. For our experiments, we incorporated a low fraction of SDPQ units, since they are intended to be exploited just as a fluorescent label. After synthesizing the polymeric backbone, the second step for the preparation of the final hydrophobically modified graft copolymers was the synthesis of amine-terminated PNIPAM and P(DMAM-*co*-NIPAM) chains using AET as chain transfer agent. The number-average molecular weight, M_n, of these chains was estimated by acid−base titration in water. As seen from the results, in Table 1, M_n values of the order of 10 kDa were obtained, in agreement with the AET/monomer molar ratio (1/100). Finally, two graft copolymers were prepared through a grafting-to reaction, using EDC as coupling agent.

All polymers were characterized by ^{1}H NMR as far as their chemical composition is concerned. The ^{1}H NMR spectra in D_2O of the P(MAA-*co*-DMA-*co*-SDPQ) backbone, the PNIPAM-NH_2 and P(DMAM-*co*-NIPAM)-NH_2 side chains, and the final graft copolymers, P(MANa-*co*-DMA-*co*-SDPQ)-*g*-PNIPAM and P(MANa-*co*-DMA-*co*-SDPQ)-*g*-P(DMAM-*co*-NIPAM) are presented in Figure 1. Concerning the P-

DOI: 10.1021/acsami.6b13161
ACS Appl. Mater. Interfaces 2016, 8, 35059−35070

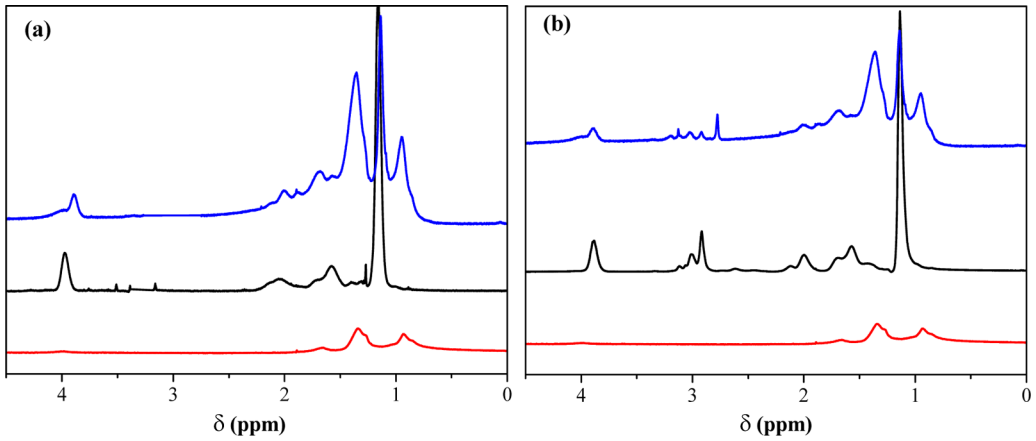

Figure 1. ^{1}H NMR spectra of (a) PNIPAM-NH_2 (black line), P(MANa-*co*-DMA-*co*-SDPQ) (red line), and P(MANa-*co*-DMA-*co*-SDPQ)-*g*-PNIPAM (blue line); and (b) P(DMAM-*co*-NIPAM)-NH_2 (black line), P(MANa-*co*-DMA-*co*-SDPQ) (red line), and P(MANa-*co*-DMA-*co*-SDPQ)-*g*-P(DMAM-*co*-NIPAM) (blue line).

(MANa-*co*-DMA-*co*-SDPQ) precursor, the peaks in the region 1.3−2.2 ppm are attributed to the methyl and methylene groups of the main polymer chain; the signal at ∼1.3 ppm corresponds to the aliphatic groups of DMA while the signal at 0.8−0.9 ppm is attributed to the characteristic peak of the $-CH_3$ groups of both MAA and DMA. Due to the low SDPQ content of the copolymers and the hydrophobic character of this unit, the protons of the quinoline groups in the region 7.5−8.0 ppm can hardly be detected in these spectra. The DMA content of the P(MAA-*co*-DMA-*co*-SDPQ) copolymers was determined from the integration ratio of the peaks at 0.8−0.9 and 1.3 ppm.

The chemical structure of the PNIPAM-NH_2 homopolymer is identified in Figure 1a, where the peaks at 3.89 and 1.15 ppm are attributed to the −CH− proton and the 6 protons of the methyl groups of isopropyl unit of PNIPAM chains, respectively. In Figure 1b, the chemical composition of the P(DMAM-*co*-NIPAM)-NH_2 copolymer was determined from the characteristic peaks at 2.9−3.3 ppm, corresponding to the 6 protons of the two $-CH_3$ groups of the PDMAM chains and the peak at 3.89, attributed to the −CH− proton of the PNIPAM chains. In the spectrum of the P(MANa-*co*-DMA-*co*-SDPQ)-*g*-PNIPAM graft copolymer in Figure 1a, the characteristic peaks of both the P(MANa-*co*-DMA-*co*-SDPQ) backbone and the PNIPAM side chains are detected. Likewise, in the case of the P(MANa-*co*-DMA-*co*-SDPQ)-*g*-P(DMAM-*co*-NIPAM) graft copolymer (Figure 1b), the peaks of the backbone and the P(DMAM-*co*-NIPAM) side chains are observed. The determination of the PNIPAM or P(DMAM-*co*-NIPAM) content of the copolymers was achieved using the peaks of the DMA, NIPAM, and DMAM units at 1.3, 3.8, and 2.9−3.3 ppm, respectively. All characterization results are summarized in Table 1.

The self-association of the resulting polymers was studied in aqueous solution by fluorescence probing using Nile Red as a fluorescence probe. Nile Red is a poorly soluble probe and is almost nonfluorescent in water. In addition, its solubility increases in less polar environments, where it is strongly fluorescent, showing an intense emission peak in the region 600−650 nm. Unfortunately, the critical micelle concentrations (CMCs) of the SDPQ-containing copolymers, namely, P(MANa-*co*-DMA-*co*-SDPQ), P(MANa-*co*-DMA-*co*-SDPQ)-*g*-PNIPAM, and P(MANa-*co*-DMA-*co*-SDPQ)-*g*-P(DMAM-*co*-NIPAM), could not be determined with this technique, possibly due to the fluorescence of the SDPQ groups. Thus, we determined the CMC of the identical P(MANa-*co*-DMA), P(MANa-*co*-DMA)-*g*-PNIPAM, and P(MANa-*co*-DMA)-*g*-P(DMAM-*co*-NIPAM) copolymers without labeling with SDPQ units.

The maximum fluorescence intensity of the emission peak of Nile Red at 600−650 nm is plotted in Figure 2 as a function of

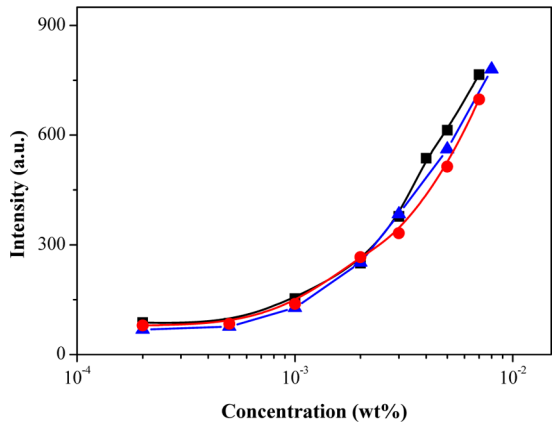

Figure 2. Dependence of the maximum fluorescence intensity of the emission of Nile Red at 600−650 nm on the polymer concentration for P(MANa-*co*-DMA) (■), P(MANa-*co*-DMA)-*g*-PNIPAM (●), and P(MANa-*co*-DMA)-*g*-P(DMAM-*co*-NIPAM) (▲).

the concentration of the copolymers. As can be observed, at low polymer concentrations, the probe detects a purely hydrophilic environment, and as a consequence the maximum intensity of Nile Red is low. However, the intensity increases sharply when the polymer concentration increases above the CMC. Apparently, the amphiphilic copolymers are now self-organized into micelles with a hydrophobic core comprising the pendent alkyl chains and a hydrophilic corona that consisted of the anionic polyelectrolyte backbone as well as the hydrophilic PNIPAM or P(DMAM-*co*-NIPAM) side chains that stabilize the system in water. As a result, the probe is now solubilized in the hydrophobic region of the formed polymeric micellar structures and "detects" a hydrophobic microenvironment. The CMC values of the copolymers are presented in Table 1. It is clear that all three copolymers exhibit the same behavior (CMC

DOI: 10.1021/acsami.6b13161
ACS Appl. Mater. Interfaces 2016, 8, 35059−35070

= 0.002 wt %), a fact that leads to the conclusion that the addition of the PNIPAM or the P(DMAM-*co*-NIPAM) side chains on the P(MANa-*co*-DMA) HMWSP does not affect the self-organization of the polymers in water. This is not surprising, since all polymers have the same backbone which controls their amphiphilic character at room temperature.

The CMC values are not expected to be significantly affected by the incorporation of such a low SDPQ content in the final copolymers. However, this SDPQ content is enough to observe the pH-responsive luminescence behavior depicted in Figure 3,

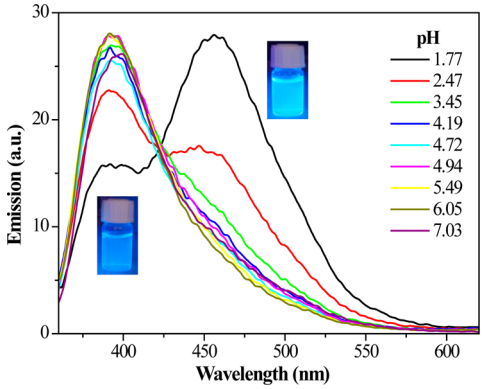

Figure 3. Emission spectra of 0.01 wt % solutions of P(MANa-*co*-DMA-*co*-SDPQ)-*g*-PNIPAM in 0.1 M buffer solutions of various pH (excitation wavelength: 350 nm).

where representative photoluminescence spectra upon excitation at 350 nm of the aqueous solution of P(MANa-*co*-DMA-*co*-SDPQ)-*g*-PNIPAM are presented. Photos of the solutions under UV irradiation at high and low pH are inserted in Figure 3. For pH ≥ 3.45, a well-defined emission peak at ∼390 nm is observed. In this case, a characteristic blue color is emitted (left photo). For lower pH values, two emission bands are observed, the blue one at 390 nm and a novel band at ∼460 nm corresponding to a green emission. This behavior is explained by the gradual protonation of the quinoline groups of SDPQ as pH decreases.[51,53] The existence of both peaks indicates that the populations of the protonated and the uncharged form of quinoline in the aqueous solution of the polymer are comparable under these conditions. The population of the protonated species decreases upon acidification, at the expense of the basic blue band at 390 nm, as revealed by the enhancement of the emission peak at 460 nm as pH decreased. However, even at pH ∼ 2, the blue band is still important, and a mixed green-blue color is observed (right photo).

The importance of the incorporation of the PNIPAM or P(DMAM-*co*-NIPAM) side chains on the P(MANa-*co*-DMA-*co*-SDPQ) backbone is shown in Figure 4. In this figure, the temperature dependence of the optical density at 500 nm of aqueous solutions of the PNIPAM and P(DMAM-*co*-NIPAM) side chains, as well as the P(MANa-*co*-DMA-*co*-SDPQ)-*g*-PNIPAM and P(MANa-*co*-DMA-*co*-SDPQ)-*g*-P(DMAM-*co*-NIPAM) graft copolymers, is demonstrated. The concentration of the NIPAM units in all solutions was fixed at 0.3 wt %. The temperature above which a homogeneous polymer solution exhibits a macroscopic phase separation and turns turbid is called the cloud point temperature (T_{CP}). The LCST can be considered as the lowest T_{CP} of the system, as it corresponds to the minimum of the phase diagram.[57] From Figure 4, the cloud points of the solutions were determined as the temperature

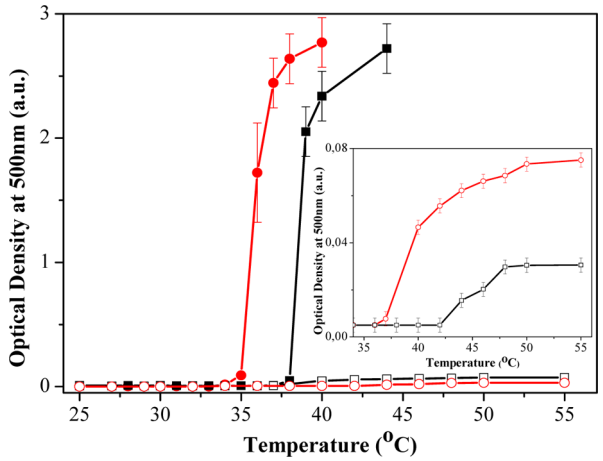

Figure 4. Optical density at 500 nm as a function of temperature for aqueous solutions (0.3 wt % in NIPAM moieties) of PNIPAM-NH_2 (■), P(DMAM-*co*-NIPAM)-NH_2 (●), P(MANa-*co*-DMA-*co*-SDPQ)-*g*-PNIPAM (□), and P(MANa-*co*-DMA-*co*-SDPQ)-*g*-P(DMAM-*co*-NIPAM) (○). Inset: Magnification of the curves of the graft copolymers.

where the optical density starts to increase abruptly, i.e., T_{CP} = 35 °C, and 38 °C for PNIPAM-NH_2 and P(DMAM-*co*-NIPAM)-NH_2 side chains, respectively. As expected, the T_{CP} of the P(DMAM-*co*-NIPAM)-NH_2 copolymer was shifted at higher temperature about 3 °C (T_{CP} = 38 °C). It should be mentioned here that an ∼18 mol % DMAM content of the copolymer was enough to slightly increase the LCST of the side grafting chains. These values are very comparable to results concerning similar P(DMAM-*co*-NIPAM) copolymers.[58,59]

As a consequence of their attachment onto the polyelectrolyte backbone, the phase separation (formation of hydrophobic domains) of the grafted PNIPAM and P(DMAM-*co*-NIPAM) side chains in water upon heating above T_{CP} is limited to the nanoscale regime.[60] Hence, the solutions of the P(MANa-*co*-DMA-*co*-SDPQ)-*g*-PNIPAM and P(MANa-*co*-DMA-*co*-SDPQ)-*g*-P(DMAM-*co*-NIPAM) copolymers are practically clear, compared to PNIPAM-NH_2 and P(DMAM-*co*-NIPAM)-NH_2, respectively. However, from the magnification of the results shown in the inset of Figure 4, the T_{CP}'s of the graft copolymers are found at 38 and 42 °C for P(MANa-*co*-DMA-*co*-SDPQ)-*g*-PNIPAM and P(MANa-*co*-DMA-*co*-SDPQ)-*g*-P(DMAM-*co*-NIPAM), respectively.

3.2. Transfer of Hydrophobic Ferrites in Water, Hyperthermia Measurements and MR Relaxivity. For the dispersion of colloidal superparticles of oleylamine-coated iron ferrite MNPs in water, the two graft copolymers P(MANa-*co*-DMA-*co*-SDPQ)-*g*-PNIPAM and P(MANa-*co*-DMA-*co*-SDPQ)-*g*-P(DMAM-*co*-NIPAM) were used. In previous reports of our group, MFe_2O_4@HMWSPs nanohybrids (where M: Co, Mn, Ni) were effectively stabilized in water through a solvent mixing procedure.[30,31] In the present work we have chosen two new polymers of a more complicated architecture to further study this concept and utilize them to disperse hydrophobic ferrite nanocrystals. Table 2 summarizes the main attempts carried out in the present work for the dispersion of colloidal superparticles. Our initial efforts focused on clustering hydrophobic manganese ferrite nanoparticles coated with oleylamine (samples MSPs1 and MSPs2). However, the main goal was the stabilization of colloidal superparticles from a mixture of $MnFe_2O_4$@OAm and

DOI: 10.1021/acsami.6b13161
ACS Appl. Mater. Interfaces 2016, 8, 35059−35070

Table 2. SLP Values of Aqueous Superparticle Dispersions

sample	metal core	copolymer	SLP (W/g)
MSPs1	$MnFe_2O_4$	P(MANa-*co*-DMA-*co*-SDPQ)-*g*-PNIPAM	36
MSPs2	$MnFe_2O_4$	P(MANa-*co*-DMA-*co*-SDPQ)-*g*-P(DMAM-*co*-NIPAM)	60
MSPs3	$MnFe_2O_4$:$CoFe_2O_4$	P(MANa-*co*-DMA-*co*-SDPQ)-*g*-PNIPAM	99
MSPs4	$MnFe_2O_4$:$CoFe_2O_4$	P(MANa-*co*-DMA-*co*-SDPQ)-*g*-P(DMAM-*co*-NIPAM)	103

$CoFe_2O_4$@OAm (1:1) MNPs (samples MSPs3 and MSPs4), aiming at the elucidation of the effect of a magnetically hard phase ($CoFe_2O_4$) on the net magnetic behavior of the superparticles. Primarily, nanoparticles ($MnFe_2O_4$ and $CoFe_2O_4$) were synthesized under solvothermal conditions by our group, using oleylamine in a triple role (solvent and reducing and surface-functionalizing agent).[45,46] The as-synthesized nanocrystals were 9 nm in size and highly uniform while they were very well-dispersed in nonpolar organic solvents, forming very stable colloids. For the convenience of the reader, basic characterization of the primary ferrite nanoparticles is given at Supporting Information (Figures S1−S4), while further information can be found elsewhere.[45,46]

Representative TEM images of the spherical nanostructures stabilized in water, above the CMC of the copolymers, of MNP@P(MANa-*co*-DMA-*co*-SDPQ)-*g*-PNIPAM and MNP@P(MANa-*co*-DMA-*co*-SDPQ)-*g*-P(DMAM-*co*-NIPAM) (where MNP = $MnFe_2O_4$@OAm or a 1:1 mixture of $MnFe_2O_4$@OAm/$CoFe_2O_4$@OAm MNPs) are presented in Figure 5. As can be seen in Figure 5a,c, the hydrophobic $MnFe_2O_4$@OAm MNPs are located in the hydrophobic DMA core of the micelles formed by the two copolymers above their CMC. A similar behavior is also exhibited when a mixture of $MnFe_2O_4$@OAm/$CoFe_2O_4$@OAm MNPs is used (Figure 5b,d). In the TEM images, the hydrophilic corona of the micelles, comprised by the hydrophilic MANa groups and the PNIPAM and P(DMAM-*co*-NIPAM) side chains, cannot be seen due to the high contrast of the MNPs. It is noteworthy that the size of the cores of the nanohybrids takes values below 100 nm. The samples MSPs1, MSPs3, and MSPs4 comprise clusters of similar morphology in contrast to MSPs2 where isolated nanoparticles and clusters with broad size distribution are present. Indicative size distributions and hydrodynamic diameters of the prepared superparticles are shown in Supporting Information (Figures S5 and S6).

The composition of the mixed superparticles ($MnFe_2O_4$@OAm/$CoFe_2O_4$@OAm) was verified by SEM which can provide elemental map images and EDS spectra (Figure 6). Since superparticles are ultrasmall, an elemental map image of each individual cluster could not be obtained. Therefore, we provide overall elemental map images of superparticles. As expected, identical elemental map images for Mn and Co in each sample are observed, implying that nanoparticles are mixed within each cluster. Furthermore, the relative atomic abundance (%) of the different constituents (Mn, Co and Fe) obtained from the EDS spectra reveals similar concentrations of manganese (19.96%) and cobalt (19.43%) while iron was found as a major component (80.16%), certifying thus the generic formula.

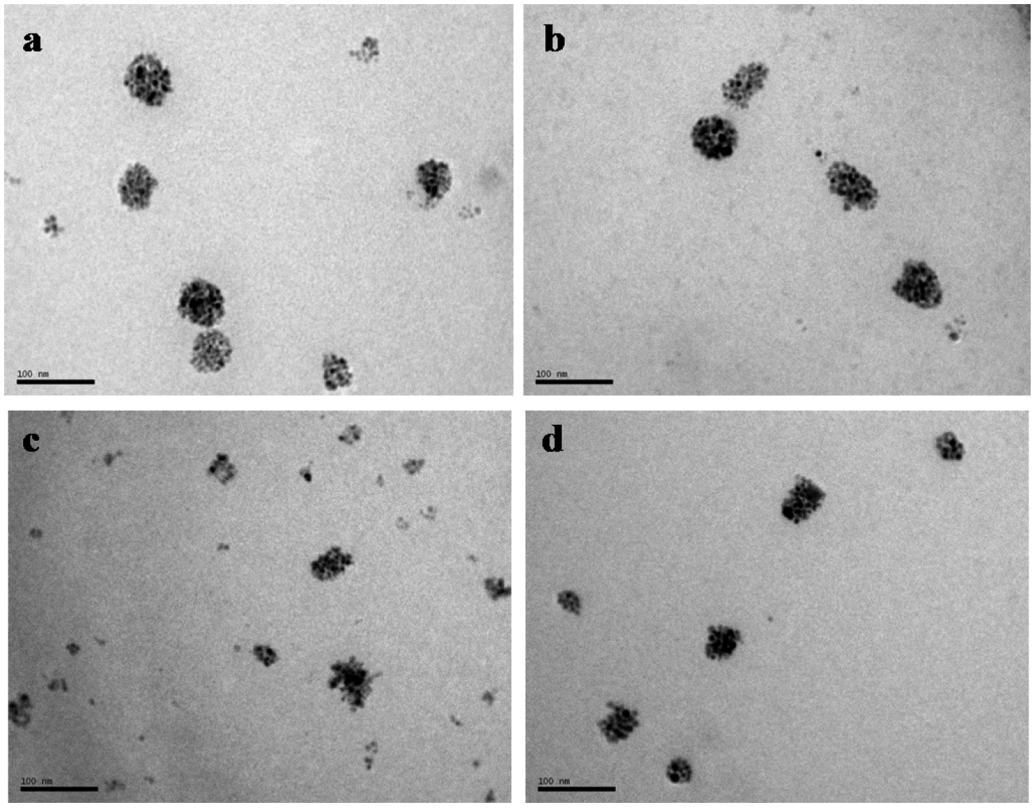

Figure 5. TEM images of (a) $MnFe_2O_4$@P(MANa-*co*-DMA-*co*-SDPQ)-*g*-PNIPAM, (b) $MnFe_2O_4$:$CoFe_2O_4$(1:1)@P(MANa-*co*-DMA-*co*-SDPQ)-*g*-PNIPAM, (c) $MnFe_2O_4$@P(MANa-*co*-DMA-*co*-SDPQ)-*g*-P(DMAM-*co*-NIPAM), and (d) $MnFe_2O_4$:$CoFe_2O_4$(1:1)@P(MANa-*co*-DMA-*co*-SDPQ)-*g*-P(DMAM-*co*-NIPAM). Scale bar: 100 nm.

DOI: 10.1021/acsami.6b13161
ACS Appl. Mater. Interfaces 2016, 8, 35059−35070

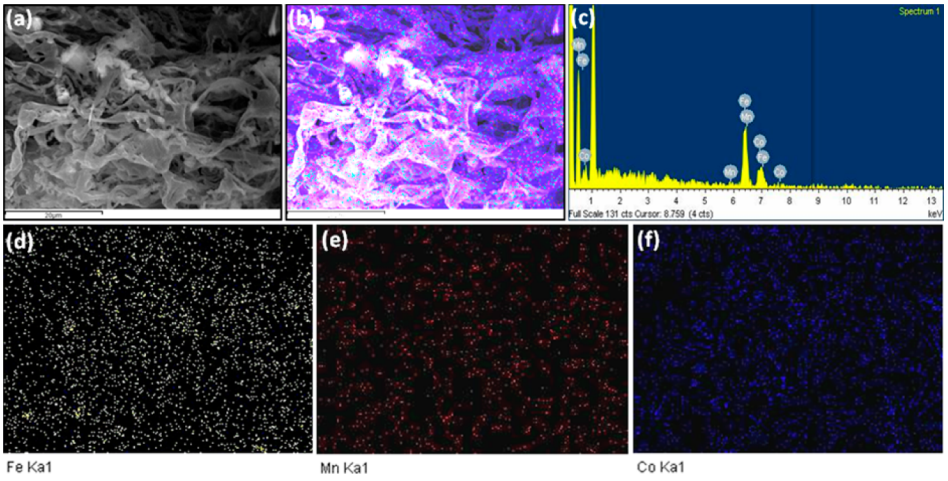

Figure 6. Elemental map images at 20 μm scale (a, b) and EDS spectrum (c). Distribution of iron element (d), distribution of manganese element (e), and distribution of cobalt element (f).

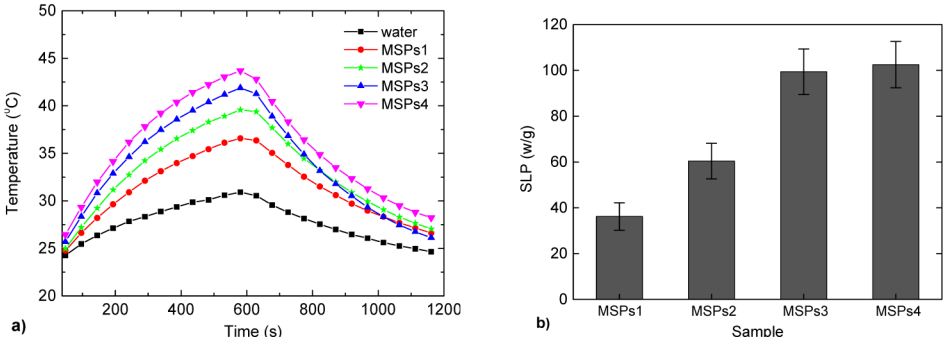

Figure 7. (a) Temperature versus time curves and (b) SLP values of the samples.

In order to assess the efficacy of the colloidal superparticles as hyperthermia agents, magnetic heating profiles were carried out under a 765 kHz alternating magnetic field with an amplitude of 250 Oe. The metal concentration of the four samples was fixed at 2 mg/mL. The temperature variation with the time of exposure to magnetic field is shown in Figure 7a. After 10 min, the temperature rises to 35 °C (lower than the body temperature) for sample MSPs1 (the side chains are consisted by the homopolymer PNIPAM), and 37 °C (around body temperature) for sample MSPs2 (the side chains are consisted by the copolymer P(DMAM-*co*-NIPAM)), while temperature increases above body temperature, 40 and 44 °C, for samples composed by the mixed superparticles, MSPs3 and MSPs4, respectively. The latter temperatures, especially that obtained for the sample MSPs4 (mixed superparticles stabilized by the copolymer containing the P(DMAM-*co*-NPAM) side chains), are optimal for conventional hyperthermia treatment.[4,61,62]

The specific loss power (SLP), or usually denoted specific absorption rate (SAR), of the four samples is shown in Figure 7b and reported in Table 2. As can be seen, the SLP values are quite different for the samples MSPs1 and MSPs2 which consist of the same metal core, while those for MSPs3 and MSPs4 are significantly increased. Concerning MSPs1 and MSPs2, SLP differences stem from an insufficient clustering process in the case of MSPs2 rather than the polymer type involved as the cloud point has not been reached for both samples. This different morphology (MSPs2) is shown by the presence of single nanoparticles together with a number of smaller clusters, as depicted in TEM images (Figure 5c), indicated also by the broader size distribution found from DLS measurements (Figure S6c). Although the increment is not significant (given the error bar), it is possible that, in the presence of small clusters (<20 nm) and a low viscosity medium (water), Brownian relaxation could be activated enhancing a further heating effect.[63,64] In general, Brownian physical rotation is one of the three dominant mechanisms for heating while the other two are Néel relaxation and hysteresis loss.[46,65] Superparticles of large hydrodynamic diameters (~50 nm) do not show Brownian effects, especially at high frequency such as that at 765 kHz used in our experiments. However, the presence of Co-ferrite NPs (MSPs3 and MSPs4) inserts an extra mechanism for heating, which is derived from hysteresis losses due to anisotropy of cobalt.[31,45] Thus, the best SLP values are obtained for MSPs3 and MSPs4, where clusters are formed by Co-ferrite and Mn-ferrite NPs. In the case of samples MSPs1 and MSPs2, which consisted only of manganese ferrite NPs, the role of the polymer type is not profound since the cloud points are not reached during hyperthermia measurements. On the contrary, in the mixed samples MSPs3 and MSPs4, the temperature overcame the cloud point for both samples. Therefore, these systems can be further exploited as theranostic agents (e.g., releasing drug from their interior simultaneously to heat treatment). In this case, the composition of the side chains is crucial, since it allows the fine-tuning of temperature for such potential applications. If we neglect particle−particle interactions, as a similar composition has been found for both samples, we assume that hysteresis losses and Néel relaxation

DOI: 10.1021/acsami.6b13161
ACS Appl. Mater. Interfaces 2016, 8, 35059−35070

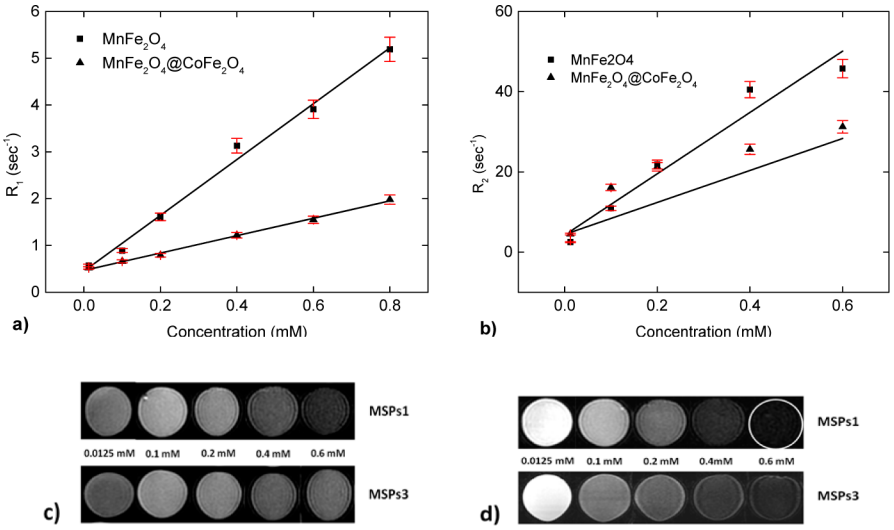

Figure 8. (a) R_1 and (b) R_2 relaxation plots of aqueous suspensions of the samples as a function of concentration, and (c) T1- and (d) T2-weighted MR images of different concentrations, respectively.

are the dominant heating mechanisms. Even though a direct comparison of SLP data is not always accurate, as different field parameters can be used, similar results have been recently reported.[36,66,67] For instance, $MnFe_2O_4$-loaded polymer nanospheres (~100 nm) showed a heating efficacy of 102 W/g under different experimental conditions (435 MHz, 4 kA m^{-1}),[66] while the SLP values of Fe_3O_4 nanoclusters (40 nm) were found to be 39.22 and 92.62 W/g with an applied field of 8.82 and 10.0 kA/m, respectively (at a fixed frequency of 425 kHz).[67] Higher SLP value (149.2 W/g) as expected due to bigger size has been indicated for core/shell microspheres (140 nm) of Fe_3O_4/carbon/PNIPAM under a field of 230 kHz and 23 kAm^{-1}.[36] Although a relatively high frequency has been applied, leading to a rather high product of the field frequency and amplitude (~2 × 10^{10} Am^{-1} s^{-1}, larger than ~5 × $10^8 Am^{-1}s^{-1}$, which is the estimated threshold for major discomfort), analogous protocols are currently examined as alternatives to overcome the usual constraints of limited heat efficacy.[68,69] In addition, we have examined our experimental sequence in vitro, and it was found that it is very well-penetrated by normal and cancer cell lines.[70] Moreover, the system can be effectively optimized as it concerns the macromolecular design (molecular weight of the backbone and the graft chains, grafting density) and the nanoparticles (size of nanoparticles, mixing ratios), aiming at higher SLP values.

In order to evaluate the performance of these nanoclusters as a possible bifunctional system for simultaneous hyperthermia and imaging applications, 1.5 T MRI studies were performed to investigate their relaxivities (r_1 and r_2) as contrast agents. From the two polymers, we have chosen the copolymer with the lower T_{CP} (38 °C), i.e., P(MANa-*co*-DMA-*co*-SDPQ)-*g*-PNIPAM, for these studies. The shrinkage of the side chains above 38 °C offers the extra ability to release incorporated drugs from the interior of the nanostructure, and therefore, these systems could be used as theranostic agents, potentially allowing simultaneous detection and treatment of cancer by hyperthermia. Figure 8a,b shows the transverse relaxation rates (R_1 and R_2) for various metal concentrations of the superparticles, while the obtained r_1 and r_2 values and relaxation ratio (r_2/r_1) are presented in Table 3. It can be observed that

Table 3. Relaxivities and Relaxation Ratio of Superparticles Measured at 1.5 T

sample	metal core	r_1 (mM^{-1} s^{-1})	r_2 (mM^{-1} s^{-1})	r_2/r_1
MSPs1	$MnFe_2O_4$	5.96	76.43	12.82
MSPs3	$MnFe_2O_4$:$CoFe_2O_4$	1.85	39.87	21.55

both r_1 and r_2 relaxivities for MSPs1 are higher than those of MSPs3, whereas an opposite trend is observed in the relaxation ratios. The decrease of relaxivities in MSPs3 can be attributed to the presence of cobalt ferrite nanoparticles which are characterized as ferromagnetic particles and are not able to rotate their magnetization as fast as the superparamagnetic manganese ferrite NPs. The high r_2/r_1 value for both systems indicates that samples are suitable for T_2-weighted MRI imaging. Finally, T1- and T2-weighted phantom MRI images were obtained at a series of colloidal suspension of nanoclusters. As shown in Figure 8, the T_2-weighted phantom images of MSPs1 exhibited a significant negative dose dependent contrast enhancement, suggesting that nanoassemblies are very promising for theranostic purposes. Even though sample MSPs3 did not reveal effective contrast sensitivity, it can be still considered as a theranostic candidate taking into account that common clinical MRI scanners usually operate at higher field (at least 3 T).

4. CONCLUSIONS

We have demonstrated the effective encapsulation and dispersion in aqueous media of hydrophobic ferrite nanoparticles as colloidal magnetic superparticles (MSPs) with multifunctional and responsive characteristics, taking advantage of multiresponsive copolymers comprising a hydrophobically modified water-soluble backbone, grafted with thermoresponsive NIPAM-based side chains. The copolymers possess pH-responsive luminescent properties stemming from SDPQ units, while the attachment of PNIPAM or P(DMAM-*co*-NIPAM) side chains resulted in different T_{CP} temperatures, close or slightly above body temperature. It is found that the effective heating characteristics of the formed nanoassemblies depend on the composition of the metal core. When $CoFe_2O_4$ particles were mixed with $MnFeO_4$ in equal amounts, SLP values

DOI: 10.1021/acsami.6b13161
ACS Appl. Mater. Interfaces 2016, 8, 35059−35070

increased significantly proving that the inset of particles with high anisotropy is of key importance for hyperthermia, while an opposite trend was observed in the MRI studies. The effective control of the inherent properties from both the organic and the inorganic materials to multifunctional inorganic−organic hybrids is very demanding. In that way our findings provide a profound and meaningful understanding of the effect of (a) the chemical structure and specific functionality of the copolymers and (b) the composition effect of the magnetic particles on the performance of the formed MSPs as hyperthermia or imaging agents. Overall, the versatility of the synthetic protocol of the novel polymeric structures presented here, in combination with the advantages of mixed magnetic nanoparticles, allows the fine-tuning and optimization of desired features (responsiveness to pH and temperature, pH-responsive luminescence) and functions (hyperthermia, imaging, theranostics), paving the way for a variety of clinical applications.

■ ASSOCIATED CONTENT

Supporting Information

The Supporting Information is available free of charge on the ACS Publications website at DOI: 10.1021/acsami.6b13161.

XRD patterns, fright-field images, and SAED patterns; FT-IR spectra and TGA curves of pure oleylamine and manganese/cobalt ferrite nanoparticles; hysteresis cycles of ferrite nanoparticles; and size distributions from TEM and DLS measurements (PDF)

■ AUTHOR INFORMATION

Corresponding Authors

*Phone: (+30) 2310-997876. Fax: (+30) 2310-997876. E-mail samkat@chem.auth.gr.

*Phone: (+30) 2610-997102. Fax: (+30) 2610-997122. E-mail bokias@upatras.gr.

ORCID

Georgios Bokias: 0000-0003-0893-4716

Notes

The authors declare no competing financial interest.

■ ACKNOWLEDGMENTS

This research was cofinanced by the European Union (European Social Fund-ESF) and Greek national funds through the Operational Program "Education and Lifelong Learning" of the National Strategic Reference Framework (NSRF)-Research Funding Program THALES: Investing in knowledge society through the European Social Fund. The authors thank Dr. Maria Kollia from the Lab of Electron Microscopy and Microanalysis at the University of Patras for the TEM images.

■ REFERENCES

(1) Lim, E.-K.; Kim, T.; Paik, S.; Haam, S.; Huh, Y.-M.; Lee, K. Nanomaterials for Theranostics: Recent Advances and Future Challenges. *Chem. Rev.* **2015**, *115*, 327−394.

(2) Kharisov, B. I.; Dias, H. V. R.; Kharissova, O. V.; Vazquez, A.; Pena, Y.; Gomez, I. Solubilization, Dispersion and Stabilization of Magnetic Nanoparticles in Water and Non-Aqueous Solvents: Recent Trends. *RSC Adv.* **2014**, *4*, 45354−45381.

(3) Dhand, C.; Dwivedi, N.; Loh, X. J.; Ying, A. N. J.; Verma, N. K.; Beuerman, R. W.; Lakshminarayanan, R.; Ramakrishna, S. Methods and Strategies for the Synthesis of Diverse Nanoparticles and their Applications: a Comprehensive Overview. *RSC Adv.* **2015**, *5*, 105003−105037.

(4) Hayashi, K.; Ono, K.; Suzuki, H.; Sawada, M.; Moriya, M.; Sakamoto, W.; Yogo, T. High-Frequency, Magnetic-Field-Responsive Drug Release from Magnetic Nanoparticle/Organic Hybrid Based on Hyperthermic Effect. *ACS Appl. Mater. Interfaces* **2010**, *2*, 1903−1911.

(5) Balasubramaniam, S.; Pothayee, N.; Lin, Y.; House, M.; Woodward, R. C.; St. Pierre, T. G.; Davis, R. M.; Riffle, J. S. Poly(N-isopropylacrylamide)-Coated Superparamagnetic Iron Oxide Nanoparticles: Relaxometric and Fluorescence Behavior Correlate to Temperature-Dependent Aggregation. *Chem. Mater.* **2011**, *23*, 3348−3356.

(6) Kim, D.-H.; Vitol, E. A.; Liu, J.; Balasubramanian, S.; Gosztola, D. J.; Cohen, E. E.; Novosad, V.; Rozhkova, E. A. Stimuli-Responsive Magnetic Nanomicelles as Multifunctional Heat and Cargo Delivery Vehicles. *Langmuir* **2013**, *29*, 7425−7432.

(7) Ye, H.; Karim, A. A.; Loh, X. J. Current Treatment Options and Drug Delivery Systems as Potential Therapeutic Agents for Ovarian Cancer: A Review. *Mater. Sci. Eng., C* **2014**, *45*, 609−619.

(8) Kakwere, H.; Leal, M. P.; Materia, M.-E.; Curcio, A.; Guardia, P.; Niculaes, D.; Marotta, R.; Falqui, A.; Pellegrino, T. Functionalization of Strongly Interacting Magnetic Nanocubes with (Thermo)-responsive Coating and their Application in Hyperthermia and Heat-Triggered Drug Delivery. *ACS Appl. Mater. Interfaces* **2015**, *7*, 10132−10145.

(9) Baek, S. M.; Singh, R. K.; Kim, T.-H.; Seo, J.-W.; Shin, U. S.; Chrzanowski, W.; Kim, H.-W. Triple Hit with Drug Carriers: pH- and Temperature-Responsive Theranostics for Multimodal Chemo- and Photothermal-Therapy and Diagnostic Applications. *ACS Appl. Mater. Interfaces* **2016**, *8*, 8967−8979.

(10) Rui, Y.-P.; Liang, B.; Hu, F.; Xu, J.; Peng, Y.-F.; Yin, P.-H.; Duan, Y.; Zhang, C.; Gu, H. Ultra-Large-Scale Production of Ultrasmall Superparamagnetic Iron Oxide Nanoparticles for T_1-Weighted MRI. *RSC Adv.* **2016**, *6*, 22575−22585.

(11) Vuong, L.; Berret, J.-F.; Fresnais, J.; Gossuin, Y.; Sandre, O. A Universal Scaling Law to Predict the Efficiency of Magnetic Nanoparticles as MRI T2-Contrast Agents. *Adv. Healthcare Mater.* **2012**, *1*, 502−512.

(12) Ge, Y.; Zhang, Y.; He, S.; Nie, F.; Teng, G.; Gu, N. Fluorescence Modified Chitosan-Coated Magnetic Nanoparticles for High-Efficient Cellular Imaging. *Nanoscale Res. Lett.* **2009**, *4*, 287−295.

(13) Chekina, N.; Horak, D.; Jendelova, P.; Trchova, M.; Benes, M. J.; Hruby, M.; Herynek, V.; Turnovcova, K.; Sykova, E. Fluorescent Magnetic Nanoparticles for Biomedical Applications. *J. Mater. Chem.* **2011**, *21*, 7630−7639.

(14) Fu, A.; Wilson, R. J.; Smith, B. R.; Mullenix, J.; Earhart, C.; Akin, D.; Guccione, S.; Wang, S. X.; Gambhir, S. S. Fluorescent Magnetic Nanoparticles for Magnetically Enhanced Cancer Imaging and Targeting in Living Subjects. *ACS Nano* **2012**, *6*, 6862−6869.

(15) Wolfbeis, O. S. An Overview of Nanoparticles Commonly Used in Fluorescent Bioimaging. *Chem. Soc. Rev.* **2015**, *44*, 4743−4768.

(16) Peng, E.; Wang, F.; Xue, J. M. Nanostructured Magnetic Nanocomposites as MRI Contrast Agents. *J. Mater. Chem. B* **2015**, *3*, 2241−2276.

(17) Na, H. B.; Song, I. C.; Hyeon, T. Inorganic Nanoparticles for MRI Contrast Agents. *Adv. Mater.* **2009**, *21*, 2133−2148.

(18) Nguyen, T.-D. From Formation Mechanisms to Synthetic Methods toward Shape-Controlled Oxide Nanoparticles. *Nanoscale* **2013**, *5*, 9455−9482.

(19) Wang, T.; Wang, X.; LaMontagne, D.; Wang, Z.; Wang, Z.; Cao, Y. C. Shape-Controlled Synthesis of Colloidal Superparticles from Nanocubes. *J. Am. Chem. Soc.* **2012**, *134*, 18225−18228.

(20) Kotov, N. A.; Tang, Z. In *Nanoparticle Assemblies and Superstructures*; Kotov, N. A., Ed.; Marcel Dekker: New York, 2005; Chapter 1.

(21) Murray, C. B.; Kagan, C. R.; Bawendi, M. G. Self-Organization of CdSe Nanocrystallites into Three-Dimensional Quantum Dot Superlattices. *Science* **1995**, *270*, 1335−1338.

(22) Talapin, D. V.; Lee, J. S.; Kovalenko, M. V.; Shevchenko, E. V. Prospects of Colloidal Nanocrystals for Electronic and Optoelectronic Applications. *Chem. Rev.* **2010**, *110*, 389−458.

(23) Dong, A.; Chen, J.; Vora, P. M.; Kikkawa, J. M.; Murray, C. B. Binary Nanocrystal Superlattice Membranes Self-Assembled at the Liquid−Air Interface. *Nature* **2010**, *466*, 474−477.
(24) Budgin, A. M.; Kabachii, Y. A.; Shifrina, Z. B.; Valetsky, P. M.; Kochev, S. S.; Stein, B. D.; Malyutin, A.; Bronstein, L. M. Functionalization of Magnetic Nanoparticles with Amphiphilic Block Copolymers: Self-Assembled Thermoresponsive Submicrometer Particles. *Langmuir* **2012**, *28*, 4142−4151.
(25) Mahajan, S.; Koul, V.; Choudhary, V.; Shishodia, G.; Bharti, A. C. Preparation and *in vitro* Evaluation of Folate-Receptor-Targeted SPION−Polymer Micelle Hybrids for MRI Contrast Enhancement in Cancer Imaging. *Nanotechnology* **2013**, *24*, 015603.
(26) Hajduová, J.; Uchman, M.; Safarik, I.; Safarikova, M.; Slouf, M.; Pispas, S.; Stepanek, M. Aggregation of Superparamagnetic Iron Oxide Nanoparticles in Dilute Aqueous Dispersions: Effect of Coating by Double-Hydrophilic Block Polyelectrolyte. *Colloids Surf., A* **2015**, *483*, 1−7.
(27) Ning, Y.; Zhang, H.; Han, J.; Yang, C.; Liu, Y.; Zhou, D.; Yang, B. Versatile Fabrication of Water-Dispersible Nanoparticle−Amphiphilic Copolymer Composite Microspheres with Specific Functionalities. *J. Mater. Chem.* **2011**, *21*, 6837−6843.
(28) Li, X.; Li, H.; Liu, G.; Deng, Z.; Wu, S.; Li, P.; Xu, Z.; Xu, H.; Chu, P. K. Magnetite-Loaded Fluorine-Containing Polymeric Micelles for Magnetic Resonance Imaging and Drug Delivery. *Biomaterials* **2012**, *33*, 3013−3024.
(29) Peng, E.; Choo, E. S. G.; Sheng, Y.; Xue, J. M. Monodisperse Transfer of Superparamagnetic Nanoparticles from Non-Polar Solvent to Aqueous Phase. *New J. Chem.* **2013**, *37*, 2051−2060.
(30) Iatridi, Z.; Georgiadou, V.; Menelaou, M.; Dendrinou-Samara, C.; Bokias, G. Application of Hydrophobically Modified Water-Soluble Polymers for the Dispersion of Hydrophobic Magnetic Nanoparticles in Aqueous Media. *Dalton Trans.* **2014**, *43*, 8633−8643.
(31) Menelaou, M.; Iatridi, Z.; Tsougos, I.; Vasiou, K.; Dendrinou-Samara, C.; Bokias, G. Magnetic Colloidal Superparticles of Co, Mn and Ni Ferrite Featured with Comb-Type and/or Linear Amphiphilic Polyelectrolytes; NMR and MRI Relaxometry. *Dalton Trans.* **2015**, *44*, 10980−10990.
(32) Hu, X.; Liu, S. Recent Advances towards the Fabrication and Biomedical Applications of Responsive Polymeric Assemblies and Nanoparticle Hybrid Superstructures. *Dalton Trans.* **2015**, *44*, 3904−22.
(33) Brazel, C. S. Magnetothermally-Responsive Nanomaterials: Combining Magnetic Nanostructures and Thermally-Sensitive Polymers for Triggered Drug Release. *Pharm. Res.* **2009**, *26*, 644−656.
(34) Shah, S. A.; Asdi, M. H.; Hashmi, M. U.; Umar, M. F.; Awan, S.-U. Thermo-Responsive Copolymer Coated $MnFe_2O_4$ Magnetic Nanoparticles for Hyperthermia Therapy and Controlled Drug Delivery. *Mater. Chem. Phys.* **2012**, *137*, 365−371.
(35) Sahoo, B.; Devi, K. S. P.; Banerjee, R.; Maiti, T. K.; Pramanik, P.; Dhara, D. Thermal and pH Responsive Polymer-Tethered Multifunctional Magnetic Nanoparticles for Targeted Delivery of Anti-Cancer Drug. *ACS Appl. Mater. Interfaces* **2013**, *5*, 3884−3893.
(36) Chen, L.; Li, L.; Zhang, H.; Liu, W.; Yang, Y.; Liu, X.; Xu, B. Magnetic Thermosensitive Core/Shell Microspheres: Synthesis, Characterization and Performance in Hyperthermia and Drug Delivery. *RSC Adv.* **2014**, *4*, 46806−46812.
(37) Patra, S.; Roy, E.; Karfa, P.; Kumar, S.; Madhuri, R.; Sharma, P. K. Dual-Responsive Polymer Coated Superparamagnetic Nanoparticle for Targeted Drug Delivery and Hyperthermia Treatment. *ACS Appl. Mater. Interfaces* **2015**, *7*, 9235−9246.
(38) Zheng, X.; Qian, J.; Tang, F.; Wang, Z.; Cao, C.; Zhong, K. Microgel-Based Thermosensitive MRI Contrast Agent. *ACS Macro Lett.* **2015**, *4*, 431−435.
(39) Heskins, M.; Guillet, J. E. Solution Properties of Poly(N-isopropylacrylamide). *J. Macromol. Sci., Chem.* **1968**, *2*, 1441−1455.
(40) Schild, H. G. Poly(N-isopropylacrylamide): Experiment, Theory and Application. *Prog. Polym. Sci.* **1992**, *17*, 163−249.
(41) Pelton, R. Temperature-Sensitive Aqueous Microgels. *Adv. Colloid Interface Sci.* **2000**, *85*, 1−33.
(42) Halperin, A.; Kroger, M.; Winnik, F. M. Poly(N-isopropylacrylamide) Phase Diagrams: Fifty Years of Research. *Angew. Chem., Int. Ed.* **2015**, *54*, 15342−15367.
(43) Hemmer, E.; Quintanilla, M.; Légaré, F.; Vetrone, F. Temperature-Induced Energy Transfer in Dye-Conjugated Upconverting Nanoparticles: A New Candidate for Nanothermometry. *Chem. Mater.* **2015**, *27*, 235−244.
(44) Menelaou, M.; Georgoula, K.; Simeonidis, K.; Dendrinou-Samara, C. Evaluation of Nickel Ferrite Nanoparticles Coated with Oleylamine by NMR Relaxation Measurements and Magnetic Hyperthermia. *Dalton Trans.* **2014**, *43*, 3626−3636.
(45) Vamvakidis, K.; Katsikini, M.; Sakellari, D.; Paloura, E. C.; Kalogirou, O.; Dendrinou-Samara, C. Reducing the Inversion Degree of $MnFe_2O_4$ Nanoparticles through Synthesis to Enhance Magnetization: Evaluation of their ^1H NMR Relaxation and Heating Efficiency. *Dalton Trans.* **2014**, *43*, 12754−12765.
(46) Georgiadou, V.; Kokotidou, C.; Le Droumaguet, B.; Carbonnier, B.; Choli-Papadopoulou, T. C.; Dendrinou-Samara, C. Oleylamine as a Beneficial Agent for the Synthesis of $CoFe_2O_4$ Nanoparticles with Potential Biomedical Uses. *Dalton Trans.* **2014**, *43*, 6377−6388.
(47) Lu, L.; Jenekhe, S. Poly(vinyl diphenylquinoline): A New pH-Tunable Light-Emitting and Charge-Transport Polymer Synthesized by a Simple Modification of Polystyrene. *Macromolecules* **2001**, *34*, 6249−6254.
(48) Jenekhe, S.; Lu, L.; Alam, M. New Conjugated Polymers with Donor−Acceptor Architectures: Synthesis and Photophysics of Carbazole−Quinoline and Phenothiazine−Quinoline Copolymers and Oligomers Exhibiting Large Intramolecular Charge Transfer. *Macromolecules* **2001**, *34*, 7315−7324.
(49) Moutsiopoulou, A.; Andreopoulou, A. K.; Lainioti, G.; Bokias, G.; Voyiatzis, G.; Kallitsis, J. K. Quinoline-Functionalized Cross-Linked Poly(vinyl acetate) and Poly(vinyl alcohol) Nanoparticles as Potential pH-Responsive Luminescent Sensors. *Sens. Actuators, B* **2015**, *211*, 235−244.
(50) Thivaios, I.; Kakogianni, S.; Bokias, G. A Library of Quinoline-Labeled Water-Soluble Copolymers with pH Tunable Fluorescence Response in the Acidic pH Region. *Macromolecules* **2016**, *49*, 3526−3534.
(51) Thivaios, I.; Diamantis, I.; Bokias, G.; Kallitsis, J. K. Temperature-Responsive Photoluminescence of Quinoline-Labeled Poly(N-isopropylacrylamide) in Aqueous Solution. *Eur. Polym. J.* **2012**, *48*, 1256−1265.
(52) Thivaios, I.; Koukoumtzis, V.; Kallitsis, J. K.; Bokias, G. Quinoline-Labeled Poly(N-isopropylacrylamide): A Selective Polymeric Luminescent Sensor of Cationic Surfactants. *Sens. Actuators, B* **2016**, *233*, 127−135.
(53) Economopoulos, S.; Andreopoulou, A.; Gregoriou, V.; Kallitsis, J. K. Synthesis and Optical Properties of New End-Functionalized Polyquinolines. *Chem. Mater.* **2005**, *17*, 1063−1071.
(54) Durand, A.; Hourdet, D. Synthesis and Thermoassociative Properties in Aqueous Solution of Graft Copolymers Containing Poly(N-isopropylacrylamide) Side Chains. *Polymer* **1999**, *40*, 4941−4951.
(55) Mamiya, H.; Jeyadevan, B. Optimal Design of Nanomagnets for Targeted Hyperthermia. *J. Magn. Magn. Mater.* **2011**, *323*, 1417−1422.
(56) Simeonidis, K.; Martinez-Boubeta, C.; Balcells, Ll.; Monty, C.; Stavropoulos, G.; Mitrakas, M.; Matsakidou, A.; Vourlias, G.; Angelakeris, M. Fe-Based Nanoparticles as Tunable Magnetic Particle Hyperthermia Agents. *J. Appl. Phys.* **2013**, *114*, 103904−8.
(57) Durand, A.; Hourdet, D. Thermoassociative Graft Copolymers Based on Poly(N-isopropylacrylamide): Effect of Added Co-Solutes on the Rheological Behavior. *Polymer* **2000**, *41*, 545−557.
(58) Pagonis, K.; Bokias, G. Simultaneous Lower and Upper Critical Solution Temperature-Type Co-Nonsolvency Behaviour Exhibited in Water−Dioxane Mixtures by Linear Copolymers and Hydrogels Containing *N*-isopropylacrylamide and *N*,*N*-dimethylacrylamide. *Polym. Int.* **2006**, *55*, 1254−1258.
(59) Liu, X.-M.; Yang, Y.-Y.; Leong, K. W. Thermally Responsive Polymeric Micellar Nanoparticles Self-Assembled from Cholesteryl

DOI: 10.1021/acsami.6b13161
ACS Appl. Mater. Interfaces 2016, 8, 35059−35070

End-Capped Random Poly(N-isopropylacrylamide-co-N, N-dimethylacrylamide): Synthesis, Temperature-Sensitivity, and Morphologies. *J. Colloid Interface Sci.* **2003**, *266*, 295−303.
(60) Durand, A.; Hourdet, D.; Lafuma, F. Thermoassociative Graft Copolymers: NMR Investigation and Comparison with Rheological Behaviour. *J. Phys. Chem. B* **2000**, *104*, 9371−9377.
(61) Jordan, A.; Scholz, R.; Wust, P.; Fahling, H.; Felix, R. Magnetic Fluid Hyperthermia (MFH): Cancer Treatment with AC Magnetic Field Induced Excitation of Biocompatible Superparamagnetic Nanoparticles. *J. Magn. Magn. Mater.* **1999**, *201*, 413−419.
(62) Ito, A.; Shinkai, M.; Honda, H.; Kobayashi, T. Medical Application of Functionalized Magnetic Nanoparticles. *J. Biosci. Bioeng.* **2005**, *100*, 1−15.
(63) Deatsch, A. E.; Evans, B. A. Heating Efficiency in Magnetic Nanoparticle Hyperthermia. *J. Magn. Magn. Mater.* **2014**, *354*, 163−172.
(64) Mazarío, E.; Sánchez-Marcos, J.; Menéndez, N.; Cañete, M.; Mayoral, A.; Rivera-Fernández, S.; de la Fuente, J. M.; Herrasti, P. *J. Phys. Chem. C* **2015**, *119*, 6828−6834.
(65) Liu, X. L.; Fan, H. M.; Yi, J. B.; Yang, Y.; Choo, E. S. G.; Xue, J. M.; Fan, D. D.; Ding, J. Optimization of Surface Coating on Fe_3O_4 Nanoparticles for High Performance Magnetic Hyperthermia Agents. *J. Mater. Chem.* **2012**, *22*, 8235−8244.
(66) Liu, X. L.; Choo, E. S. G.; Ahmed, A. S.; Zhao, L. Y.; Yang, Y.; Ramanujan, R. V.; Xue, J. M.; Fan, D. D.; Fan, H. M.; Ding, J. Magnetic Nanoparticle-Loaded Polymer Nanospheres as Magnetic Hyperthermia Agents. *J. Mater. Chem. B* **2014**, *2*, 120−128.
(67) Barick, K. C.; Aslam, M.; Lin, Y.-P.; Bahadur, D.; Prasad, P. V.; Dravid, V. P. Novel and Efficient MR Active Aqueous Colloidal Fe_3O_4 Nanoassemblies. *J. Mater. Chem.* **2009**, *19*, 7023−7029.
(68) Kozissnik, B.; Bohorquez, A. C.; Dobson, J.; Rinaldi, C. Magnetic fluid hyperthermia: Advances, challenges, and opportunity. *Int. J. Hyperthermia* **2013**, *29*, 706−714.
(69) Laurent, S.; Forge, D.; Port, M.; Roch, A.; Robic, C.; Vander Elst, L.; Muller, R. N. Magnetic Iron Oxide Nanoparticles: Synthesis, Stabilization, Vectorization, Physicochemical Characterizations, and Biological Applications. *Chem. Rev.* **2008**, *108*, 2064−2110.
(70) Chalkidou, A.; Simeonidis, K.; Angelakeris, M.; Samaras, T.; Martinez-Boubeta, C.; Balcells, L.; Papazisis, K.; Dendrinou-Samara, C.; Kalogirou, O. In vitro application of Fe/MgO nanoparticles as magnetically mediated hyperthermia agents for cancer treatment. *J. Magn. Magn. Mater.* **2011**, *323*, 775−780.

DOI: 10.1021/acsami.6b13161
ACS Appl. Mater. Interfaces 2016, 8, 35059−35070